Journal of Geophysical Research: Solid Earth

Supporting Information for

Impact of Inherited Geometries on Syn-orogenic Foreland Basin Architecture

B. Gérard[1], D. Rouby[1], R. S. Huismans[2], C. Robin[3], C. Fillon[4] and J. Braun[5,6]

[1]GET, Université de Toulouse, CNRS, IRD, UPS, Toulouse, France

[2]Department of Earth Sciences, Bergen University, Norway

[3]CNRS, Géosciences Rennes, UMR6118, University of Rennes, Rennes, 35042, France

[4]TotalEnergies, Centre Scientifique et Technique Jean Féger, Avenue Larribau, 64018 Pau Cédex, France

[5]Helmholtz Centre Potsdam, German Research Centre for Geosciences, Potsdam, Germany

[6]Institute of Geosciences, University of Potsdam, Potsdam, Germany

Contents of this file

Additional Supporting Information

Movie S4. Topographic and bathymetric evolution of the experiment M4 for 25 Myr.

Introduction

We present hereafter the equations which govern the continental and marine landscapes evolution implemented in FastScape (Text S1). We also provide additional results for experiments M2, M3 and M4: evolution through time of topography/bathymetry and depositional depth (Figures S1 to S3; Movies S2 to S4). Figure S4 presents onshore erosion/deposition rates for experiments M1 to M4. Figure S5 shows the depositional slope in the foreland through time for experiments M1 to M4 which allowed to extract the boundary between fluvial plain and alluvial fan deposits for Figures 6, 8 and 9. Figures S6 to S8 show mountain range and proximal foreland basin erosion and deposition rates evolution focusing on timings related to changes in the depositional environments at the foot of the mountain range associated with high variabilities in erosion rates (respectively for models M2 to M4). Figures S9 to S11 show sensitivity analysis of experiment M1 setup to various uplift rates (U), erodibilities (Kf) and effective elastic thicknesses (EET) respectively (Text S2; Table S1).

Text S1. Equations processed in FastScape.

We use the landscape evolution model (LEM) FastScape S2S (https://github.com/fastscape-lem/fastscapelib-fortran; (Yuan et al., 2019a; Yuan et al., 2019b). The version of the program we use is the one published online on April 26th 2021 (release v0.1.0beta3; fastscapelib-fortran; public access) available on GitHub: https://github.com/fastscape-lem. The program has been built to describe the evolution of a fluvial landscape, including sediment production by erosion, transport and deposition as well as the marine deposition in domains below sea-level (Yuan et al., 2019a; Yuan et al., 2019b). Onland relief variation are driven by the following equation 1:

$$\frac{\delta h}{\delta t} = U - K_f A^m S^n + K_h \nabla^2 h + \frac{G}{A}\int_A (U - \frac{\delta h}{\delta t}) dA \qquad \text{Equation 1}$$

in which $\frac{\delta h}{\delta t}$ is the rate of change of topography in continental domains, h is the elevation, t is the time, U is the uplift or subsidence function, K_f is the erodibility coefficient, A is the upstream drainage area, m and n are the stream power law coefficients defining the concavity, S is the slope, K_h is a transport coefficient, $\nabla^2 h$ is a term that defines the slope and G is the onland deposition coefficient.

Offshore, the marine diffusion is governed by:

$$\frac{\delta h}{\delta t} = Q_s + K_d \nabla^2 h \qquad \text{Equation 2}$$

where $\frac{\delta h}{\delta t}$ is the rate of change of bathymetry, Q_s is the sediment flux coming from the continental domain at the shoreline, K_d is the marine diffusion coefficient and h is the initial bathymetry. For marine diffusion, we use a single coefficient value in the order of magnitude of a silty grain-size (Rouby et al., 2013; Simon et al., submitted; Yuan et al., 2019b).

The LEM include the flexural isostasy response to topographic and sedimentary loads. The routine uses a spectral method to solve the bi-harmonic equation governing the bending/flexure of an elastic plate floating on an inviscid fluid (the asthenosphere).

Text S2. Sensitivity analysis of experiment M1.

To test the robustness of our results, we performed a sensitivity analysis of experiment M1 to (i) various uplift rates (U; 0.1, 0.5 and 1.0 mm/yr), (ii) erodibilities (K_f; 5.0×10^{-6}, 2.5×10^{-5} and 9.0×10^{-5} $m^{0.2}$/yr) and (iii) effective elastic thicknesses (EET; 5, 15 and 25 km; Table S1; Figures S9 to S11). (i) The analysis shows that the higher the uplift rate, the higher the range topography and accordingly the topographic load, which drives higher flexural isostasy and ultimately a thicker foreland basin (Figure S9). (ii) The experiments also show that, the higher the K_f, the lower the basin basement subsidence. Indeed, higher erosion efficiency limits topography build-up in the range and, in doing so, flexure driven accommodation creation in the foreland basin (Figure S10). (iii) Finally experiments show that, the higher the EET, the higher the amplitude and the longer the wavelength of basement deepening, which produce a thicker foreland basin (Figure S11). In summary, varying uplift rate, erodibility and elastic thickness modify the timing in the basin filling dynamic and maturity stages of foreland basin. The main stratigraphic trends, as observed, described and discussed for the experiments presented in the article, do not change in this sensitivity experiments (Figures S9 to S11).

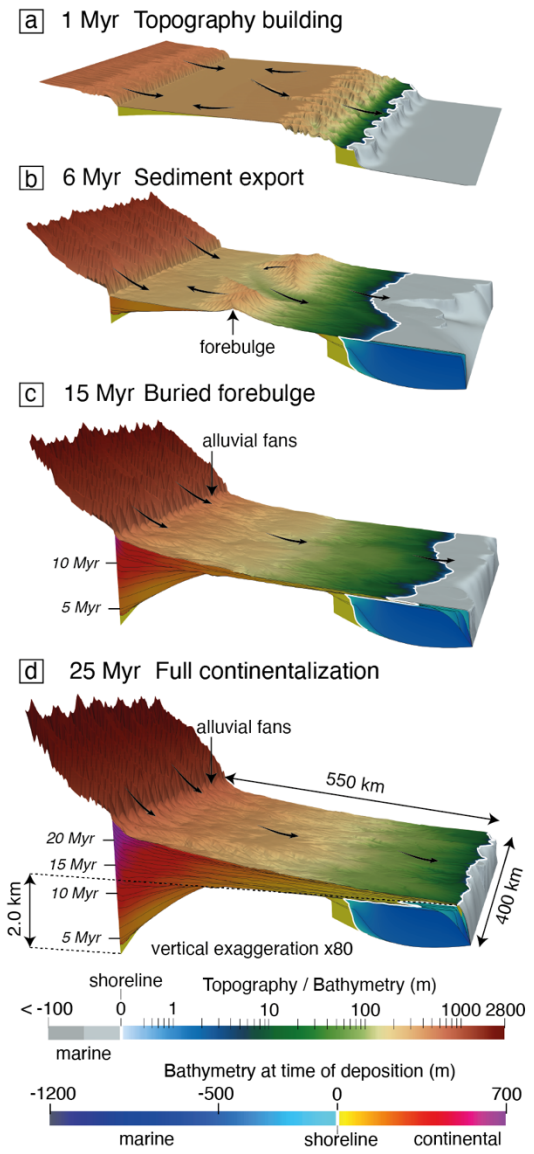

Figure S1. Evolution of M2 experiment at (a) 1 Myr; (b) 6Myr, (c) 15 Myr and (d) 25 Myr. The surface of the model is colored according to the topography/bathymetry and the section of the model according to the depositional bathymetry. Black arrows represent sediment transport directions.

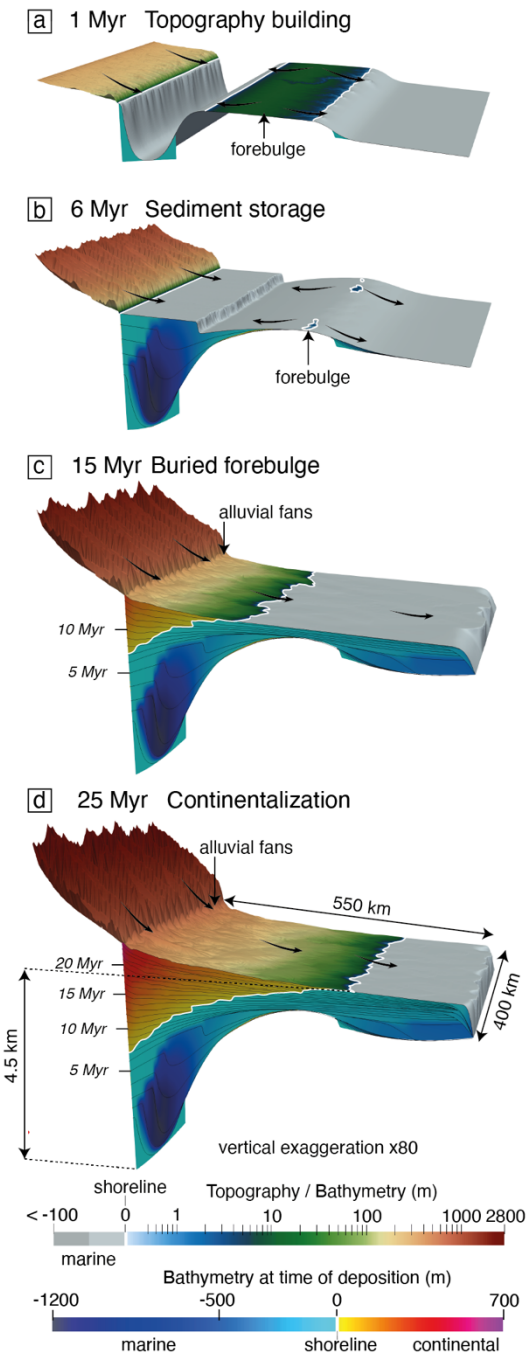

Figure S2. Evolution of M3 experiment at (a) 1 Myr; (b) 6Myr, (c) 15 Myr and (d) 25 Myr. The surface of the model is colored according to the topography/bathymetry and the section of the model according to the depositional bathymetry. Black arrows represent sediment transport directions.

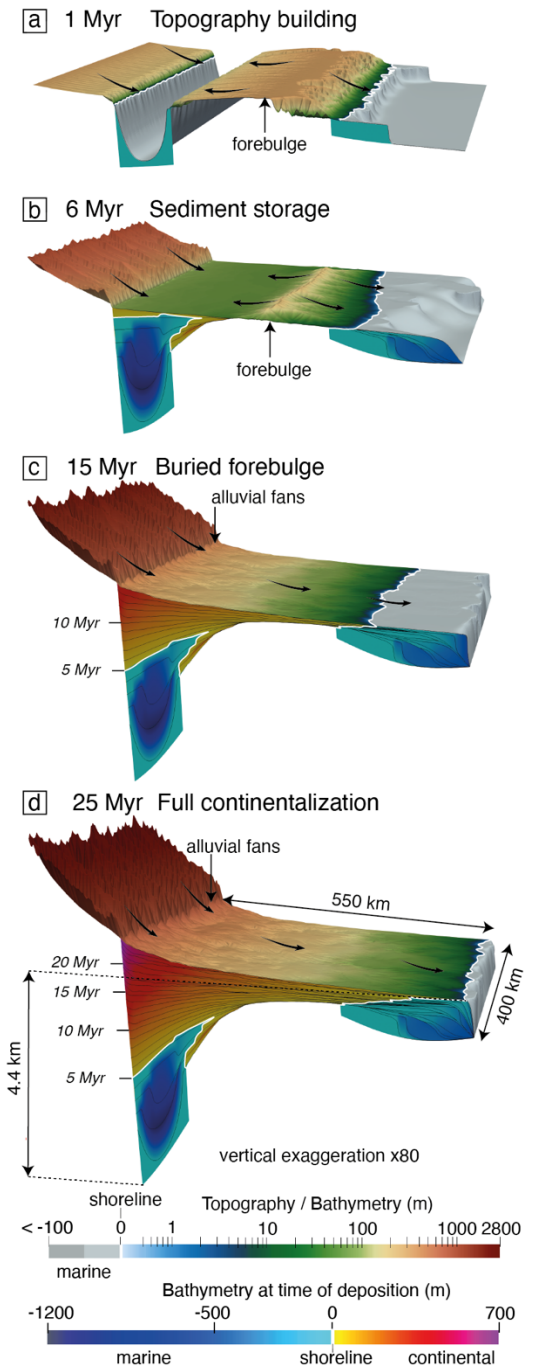

Figure S3. Evolution of M4 experiment at (a) 1 Myr; (b) 6Myr, (c) 15 Myr and (d) 25 Myr. The surface of the model is colored according to the topography/bathymetry and the section of the model according to the depositional bathymetry. Black arrows represent sediment transport directions.

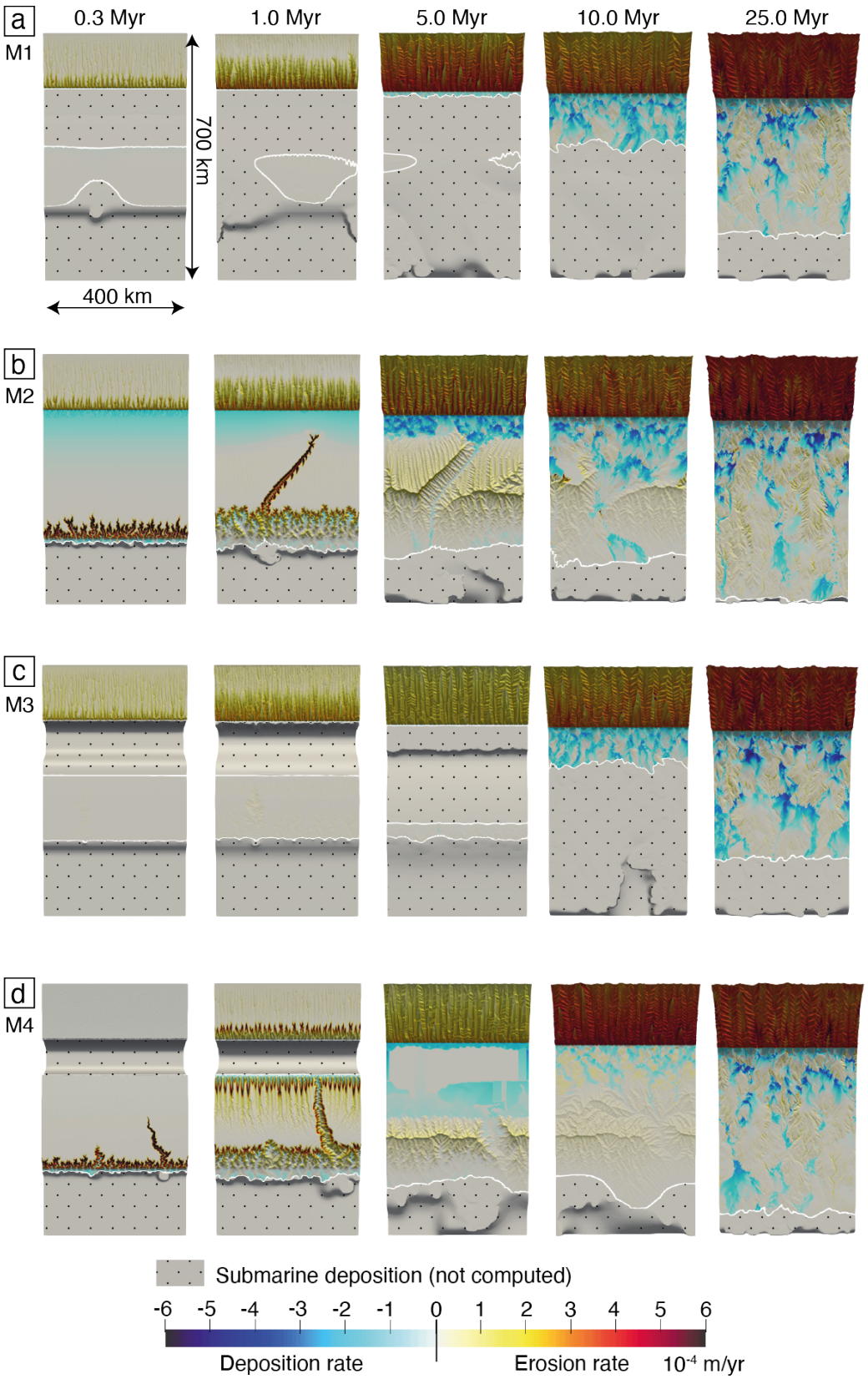

Figure S4. Top view of the deposition/erosion rate of experiments (a) M1, (b) M2, (c) M3 and (d) M4 at 0.3, 1, 5, 10 and 25 Myrs. Note that rates below sea-level are not plotted (dotted domains).

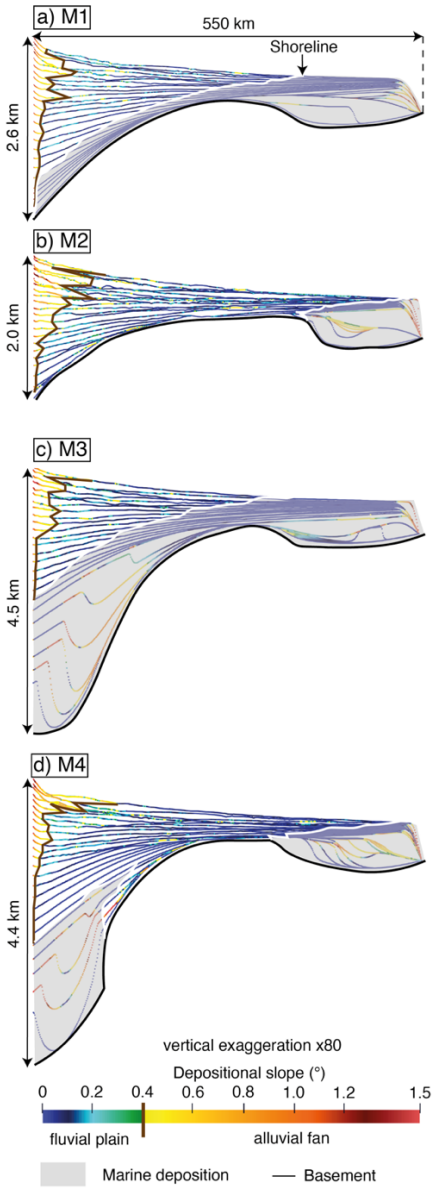

Figure S5. Depositional slopes of the sedimentary layers of experiment (a) M1, (b) M2, (c) M3 and (d) M4 (see Figure 4 for cross-section locations. Timelines are drawn every Myr. The limit between fluvial plains and alluvial fans is extracted for portions, longer than 10 km, associated to depositional slopes >0.4°. The variation of this limit through time is caused by alluvial fans lateral migration in response to the local competition between erosion and deposition (Movies S1 to S4). The general trend is nonetheless, in progradation. White lines are the shoreline.

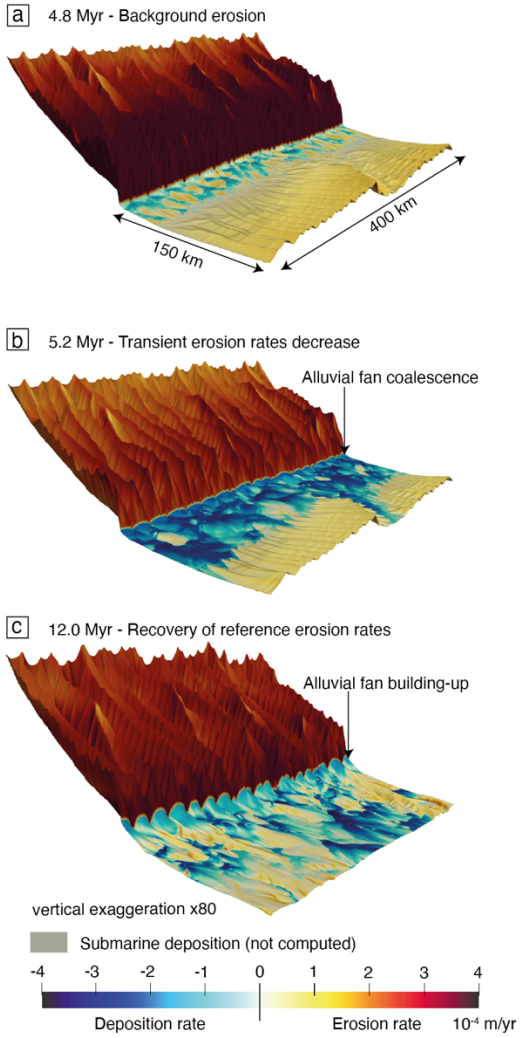

Figure S6. Zoom of the erosion and deposition rates of model M2 in the uplifted mountain range and proximal foreland domain at a) 4.8 Myr (alluvial fan build-up initiation), (b) 5.2 Myr (alluvial fan coalescence), and c) 12 Myr (after alluvial fan coalescence). Note the decrease in erosion rates in the uplifted area around 5.2 Myr.

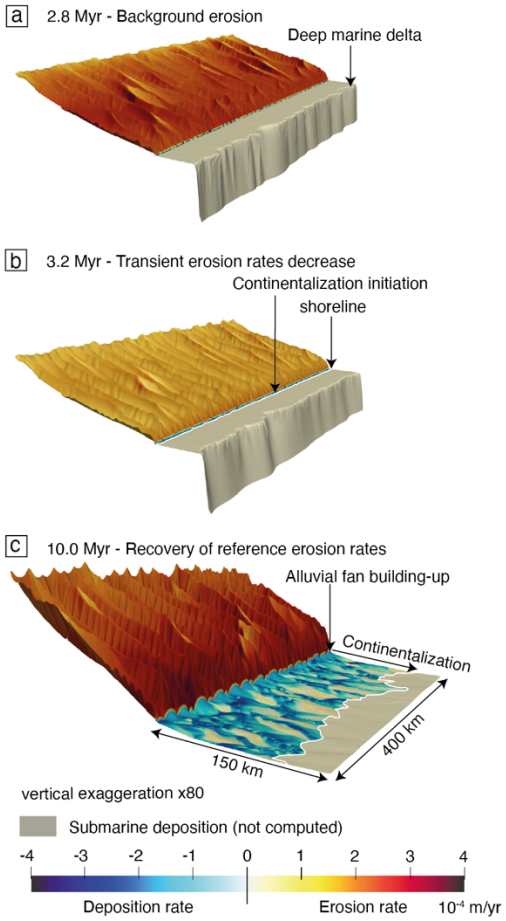

Figure S7. Zoom of the erosion and deposition rates of model M3 in the uplifted mountain range and proximal foreland domain at a) 2.8 Myr (only marine deposition in the foreland basin), (b) 3.2 Myr (continentalization initiation), and c) 10 Myr (after alluvial fan coalescence). Note the decrease in erosion rates in the uplifted area around 3.2 Myr.

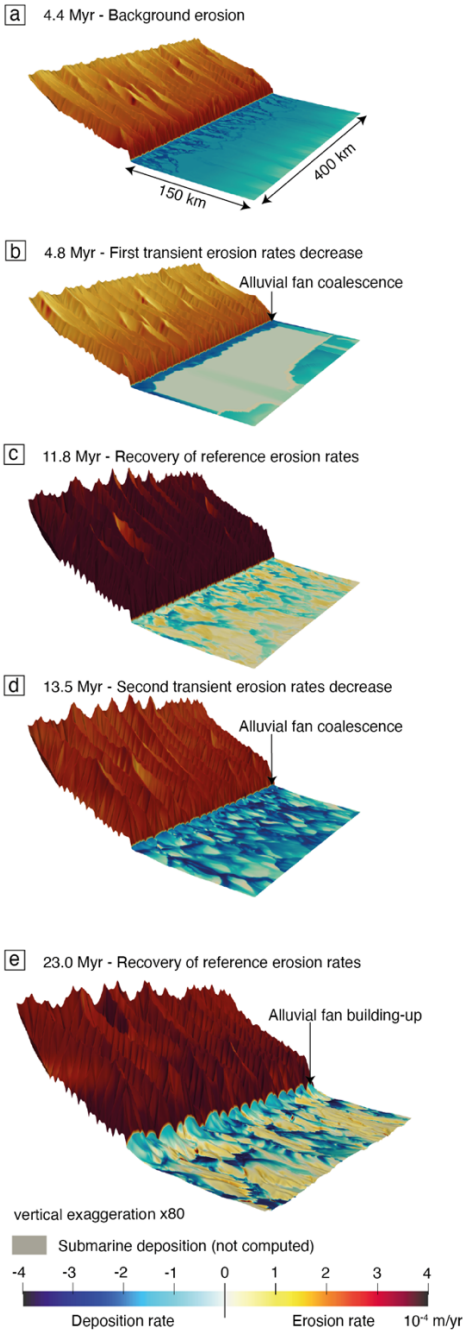

Figure S8. Zoom of the erosion and deposition rates of model M4 in the uplifted mountain range and proximal foreland domain at a) 4.4 Myr (alluvial fan build-up initiation), (b) 4.8 Myr (first alluvial fan coalescence), c) 11.8 Myr (after alluvial fan coalescence), d) 13.5 Myr (second alluvial fan coalescence), and e) 23 Myr (after alluvial fan coalescence). Note the decrease in erosion rates in the uplifted area around 4.8 and 13.5 Myr.

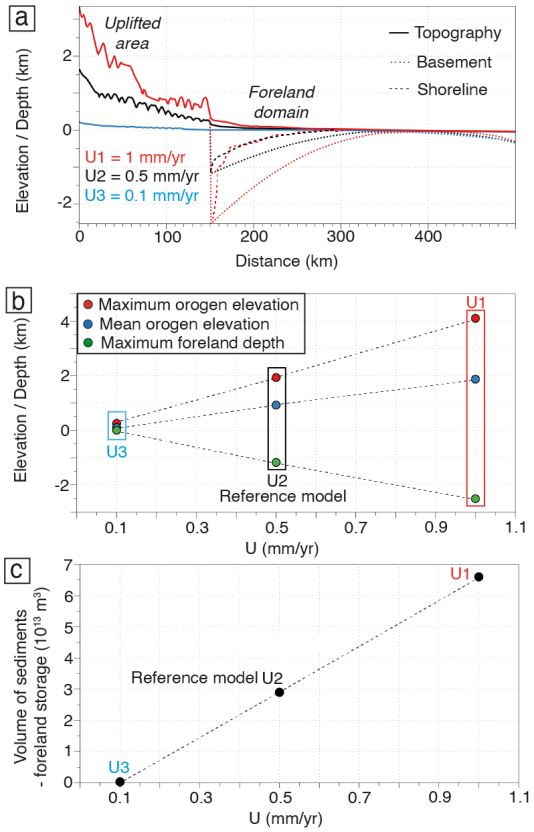

Figure S9. Sensitivity analysis of experiment M1 setup to the uplift rate (U) in the range domain. a) Cross-sections of the basement elevation/depth across at 25 Myrs for experiments with U1=1 mm/yr (Supplementary Model 1 (SM1)), U2=0.5 mm/yr (reference M1) and U3=0.1 mm/yr (SM2). b) Mountain range elevation and foreland basin maximum basement depth at 25 Myrs for U1, U2 and U3. c) Volume of sediments stored in the foreland basin at 25 Myrs for U1, U2 and U3. In the case of U3, the flexural isostasy is too small to allow foreland basin basement deepening.

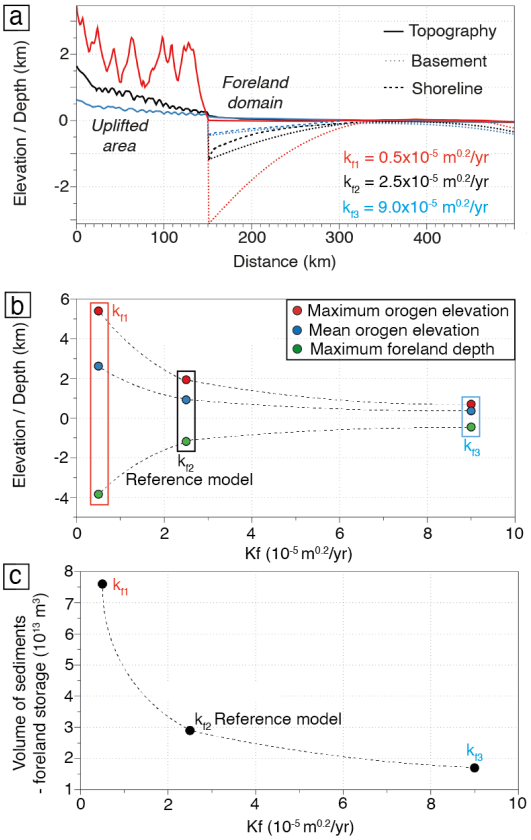

Figure S10. Sensitivity analysis of experiment M1 setup to the erodibility (k_f). a) Cross-sections of the basement elevation/depth across at 25 Myrs for experiments with k_{f1}=5x10^{-6} m$^{0.2}$/yr (Supplementary Model 3 (SM3)), k_{f2}=2.5x10^{-5} m$^{0.2}$/yr (reference M1) and k_{f3}=9x10^{-5} m$^{0.2}$/yr (SM4). b) Mountain range elevation and foreland basin maximum basement depth at 25 Myrs for k_{f1}, k_{f2} and k_{f3}. c) Volume of sediments stored in the foreland basin at 25 Myrs for k_{f1}, k_{f2} and k_{f3}. In the case of k_{f1}, foreland domain remains marine during the entire modelling process.

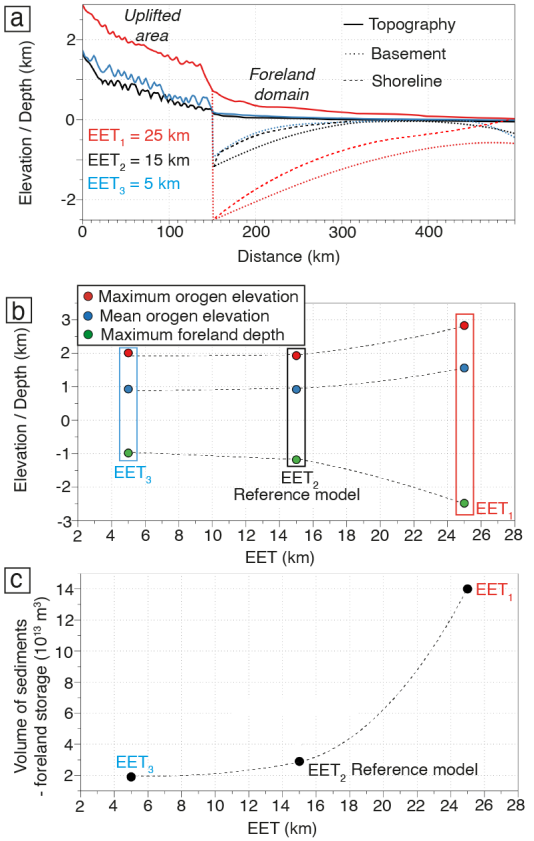

Figure S11. Sensitivity analysis of experiment M1 to the effective elastic thickness (EET). a) Cross-sections of the basement elevation/depth across at 25 Myrs for experiments with EET_1=25 km (Supplementary Model 5 (SM5)), EET_2=15 km (reference M1) and EET_3=5 km (SM6). b) Mountain range elevation and foreland basin maximum basement depth at 25 Myrs for EET_1, EET_2 and EET_3. c) Volume of sediments stored in the foreland basin at 25 Myrs for EET_1, EET_2 and EET_3. In the case of EET_3, foreland domain remains continental during the entire modelling process.

Table S1. Sensitivity Results for Reference Experiment (M1)

Parameter	Value	Unit	Mean elevation orogen 25 Myr (m)	Maximum basement depth foreland 25 Myr (m)	Volume of sediments stored in the foreland 25 Myr (10^{13} m^3)	Feedback
U	0.1	mm/yr	100	0	0.05	positive
U	0.5[a]	mm/yr	920	-1200	2.9	
U	1.0	mm/yr	1870	-2500	6.6	
K_f	5.0×10^{-6}	$m^{0.2}$/yr	2620	-3850	7.6	negative
K_f	2.5×10^{-5} [a]	$m^{0.2}$/yr	920	-1190	2.9	
K_f	9.0×10^{-5}	$m^{0.2}$/yr	360	-450	1.7	
EET	5	km	925	-980	1.9	positive
EET	15[a]	km	925	-1180	2.9	
EET	25	km	1560	-2480	14.0	

Note. U is the uplift rate, K_f is the erodibility and EET is the effective elastic thickness. See figures S9 to S11 for details regarding the sensitivity analysis. [a]Values used in reference experiment M1.

Supplementary Information references

Rouby, D., Braun, J., Robin, C., Dauteuil, O., & Deschamps, F. (2013). Long-term stratigraphic evolution of Atlantic-type passive margins: A numerical approach of interactions between surface processes, flexural isostasy and 3D thermal subsidence. *Tectonophysics*, *604*, 83–103. https://doi.org/10.1016/j.tecto.2013.02.003

Simon, B., Robin, C., Rouby, D., Braun, J., & Guillocheau, F. (n.d.). *Rifted margin stratigraphy provides calibration of marine diffusion coefficient: measurements in the Ogooué and Zambezi deltas (in revision for Basin Research)*.

Yuan, X. P., Braun, J., Guerit, L., Rouby, D., & Cordonnier, G. (2019a). A New Efficient Method to Solve the Stream Power Law Model Taking Into Account Sediment Deposition. *Journal of Geophysical Research: Earth Surface*, *124*(6), 1346–1365. https://doi.org/10.1029/2018JF004867

Yuan, X. P., Braun, J., Guerit, L., Simon, B., Bovy, B., Rouby, D., et al. (2019b). Linking continental erosion to marine sediment transport and deposition: A new implicit and O(N) method for inverse analysis. *Earth and Planetary Science Letters*, *524*, 1–15. https://doi.org/10.1016/j.epsl.2019.115728